


ORIGINAL RESEARCH ARTICLE

Application of Combined Geoelectrical Techniques for Groundwater Exploration at Federal University Gusau, Zamfara and its Environ, Northwest Nigeria

Shuaibu Ahmed Mahi 

Geology Department, Faculty of Science, Federal University Lokoja, Kogi State Nigeria

ABSTRACT

The area of study is currently facing an acute water shortage due to the dominant lithological framework that underlies the region and its fragile climate condition. As such, this study aimed at unearthing the groundwater potential of the area using a combined three geoelectrical techniques. Techniques such as Electrical Resistivity Tomography (ERT), Natural Electric Field (NEF) method, and Vertical Electrical Sounding (VES) were employed in the delineation of the groundwater potential of the area. Using an ABEM SAS-4000 Resistivity meter and a PQWT-TC150 water-detector equipment, respectively. Wenner array was employed for the conduct of ERT while Schlumberger configuration was used for VES data collection. The measured apparent resistivity value was inputted into RES2DIV software and subjected to an inversion process to generate the resistivity structural image of the subsurface. However, IP2WIN software was used for the VES data interpretation. The result of the ERT method revealed two to three geoelectrical resistivity layers: an overburdened layer of topsoil/laterite with resistivity values ranging from 6.86 Ωm to 1095 Ωm and thicknesses of 1-13 meters, a weathered/fractured basement layer, interpreted as the aquifer unit, with resistivity values between 28.7 Ωm and 345 Ωm , and thicknesses ranging from 6 - 30 meters; and a fresh/slightly fractured basement layer with resistivity values from 367 Ωm to 6899 Ωm . NEF method revealed the thickness and depth of the aquiferous layer across the six profile lines to range between 15-60m, 30-90m, 15-85m, 20-80m, 45-105m, and 20-40m respectively, with points on profile five (5) identified as the most promising site with regards to groundwater development. VES result identifies weathered and fractured layers as the major aquiferous units with resistivity values ranging from 9.965 Ωm to 9651 Ωm and 21.7 Ωm to 859 Ωm respectively with fracture thickness reaching up to 60m in some instances. The result goes in line with the outcome of both NRF and ERT techniques. The geological interference of this lithology on groundwater exploration reveals both the weathered overburden and fractured basement as aquiferous units in the study area. The study identified several promising aquiferous zones at depths ranging from 15 to 105 meters, with fractured basement layers serving as primary reservoirs for groundwater development.

ARTICLE HISTORY

Received September 03, 2024

Accepted October 31, 2024

Published November 03, 2024

KEYWORDS

Electrical Resistivity Tomography (ERT), Natural Electric Field (NEF), Vertical Electrical Sounding (VES), Groundwater Potential, Basement Complex



© The authors. This is an Open Access article distributed under the terms of the Creative Commons Attribution 4.0 License

(<http://creativecommons.org/licenses/by/4.0>)

INTRODUCTION

Due to its widespread use in urbanization, industrial growth, and domestic consumption, groundwater is now considered an essential source of Water and is thought to be free of contamination (Ojo *et al.*, 2015; Agbasi *et al.*, 2016; Hasan *et al.*, 2018; Saad *et al.*, 2012). Groundwater excavation is becoming more significant due to the increased demand for Water, especially in regions where surface water is limited as a result of climate variability (Alabi *et al.*, 2016). However, the heterogeneity of the geological terrain in a basement context makes delineating groundwater potential difficult (Akhter *et al.*, 2016; Vann *et al.*, 2020). Comprehensive hydrogeological studies are required to better understand groundwater conditions in hard rock terrain (Ogilbee *et al.*, 1973; Oladapo *et al.*, 2007;

Puttiwongrak *et al.*, 2022). Groundwater is an excellent replacement for the contaminated surface water source. Groundwater has certainly become more popular in many regions of the world these days. Water's significance cannot be emphasized because it is regarded as a resource that is necessary for life (Shuaibu *et al.*, 2022).

Groundwater is known to be present in the regolith layer and fractured bedrock of the basement rocks. Numerous hydrogeological investigations, most notably (Shuaibu *et al.*, 2022), have revealed that groundwater networks in such terrain are regulated geologic formations. However, (Olorunfemi *et al.*, 2020) argue that in these types of geological settings, an aquifer is formed by the overburden

Correspondence: Shuaibu Ahmed Mahi. Geology Department, Faculty of Science, Federal University Lokoja, Kogi State Nigeria. ✉ mahalkufr@gmail.com. Phone Number: +234 806 565 8349

How to cite: Shuaibu, A. M. (2024). Application of Combined Geoelectrical Techniques for Groundwater Exploration at Federal University Gusau, Zamfara and its Environ, Northwest Nigeria. *UMYU Scientifica*, 3(4), 244 – 259. <https://doi.org/10.56919/usci.2434.019>

that comes from the in-situ weathering of the rocks, and that aquifer is then buried beneath fractured basement rocks.

Nonetheless, the permeability, porosity, reservoir rock geometry (including overburden thickness and lateral extent), and lithology of the formation all affect an aquifer's productivity. Essentially, there is a good chance that the fractured and/or weathered bedrock sections that cover the newly formed crystalline basement complex will yield groundwater resources (Olorunfemi *et al.*, 2019).

The predominant lithology and climate of the region are the present causes of the severe water resource deficit that the Federal University Gusau campus is experiencing. The majority of the boreholes drilled in the region have relatively poor yields and are rarely able to meet the water needs of the university. This has nothing to do with the lack of comprehensive groundwater prospecting that makes use of a variety of investigative methods to identify groundwater potential.

Numerous techniques have been proposed for evaluating groundwater potential; nevertheless, the geoelectrical methodology has proven to be one of the most effective tools for delineations, having been used in numerous applications (Olorunfemi *et al.*, 2019). For instance, the most efficient and successful method for evaluating and investigating groundwater is electrical resistivity research (Zhao *et al.*, 2018; Takele *et al.*, 2019; Marere *et al.*, 2023; Nzelibe *et al.*, 2024). Electrical resistivity surveys determine the amount of target in the environment by comparing the resistivity of the target and the resistivity characteristics of the environment.

Hydrogeological research has found that Electrical Resistivity Tomography (ERT) is a valuable tool for characterizing aquifer systems. Such a technique is quite promising since it can trace lithological changes and underlying structures (Khal *et al.*, 2020). The basis of ERT is the ability to detect variations in electrical resistivity in the earth, which offers vital information on the distribution of different geological materials (Nzelibe *et al.*, 2022). Finding potential groundwater reservoirs, identifying strata with different permeabilities, and identifying lithological changes that impact aquifer systems have all been made easier with the help of this technique. ERT may fully explore the subsurface when used in conjunction with Induced Polarization (IP) techniques, providing important insights into hydrogeological dynamics that are necessary to understand the aquifer system (Hawker *et al.*, 2019). Hydrogeological exploration now makes extensive use of Electrical Resistivity Tomography (ERT) to assess subsurface structures and lithological variations.

To be more precise, ERT offers a targeted approach to mapping and assessing the electrical resistivity distribution on the ground (Chinwuko *et al.*, 2015). Through the

evaluation of resistivity variations, the identification of potential groundwater reservoirs, and the differentiation of layers with varying permeability, this method offers valuable insights into the composition of the geology. Error-prone transfer theory (ERT) can be used to investigate the intricate hydrogeological processes that are present in the aquifer system when combined with Induced Polarization (IP) methods (Ejebu & Olasehinde, 2014). Groundwater has been found for many years using a variety of geophysical techniques, either separately or in combination (Shuaibu *et al.*, 2022).

Water supply within Federal University Gusau and the environment is inadequate, taps are dry, and failure of some boreholes and fall in yield of hand-dug wells, among other water resources challenges necessitate this study. There were reports of one such shortage in the area of the Federal University Gusau Permanent site and its environs, where some university complexes had to reticulate Water far distance from the water source, or people had to walk several kilometers to fetch Water from the surface water body. However, the Water is unhygienic, making it unsafe for drinking and domestic use. The consequence is that people relying on such water bodies for their livelihood are exposed to water-related diseases thereby contributing negatively to economic activities as well as reducing their life expectancy.

With increasing water scarcity in Northwestern Nigeria, particularly around Gusau, innovative groundwater exploration techniques are essential. This study employs an integrated geophysical approach using ERT, VES, and NEF to comprehensively assess groundwater potential in the area.

MATERIALS AND METHODS

Location and Description of the Study Area

The area under investigation falls within the Nigerian Basement Complex, which lies between Latitude 12°7'15"N to 12°8'15"N and longitude 6°46'40"E to 6°47'45"E. The study area falls within Gusau sheet 54 SE. It has an area coverage of 35.4km². The study area is situated in Federal University Gusau, Bungudu local government, Zamfara State. Major settlements in the study area are Federal University Gusau and Sabon Gida. As shown in Figure 1.

Geological Setting of the Research Area

According to (Shuaibu, 2023; Eduvie and Garba, 2017), migmatite, gneiss, schist, granite, and granodiorite make up the majority of the crystalline rocks that comprise the northwest Nigerian basement complex, upon which 100% of Gusau is situated (Figure 2). They display structural characteristics such as joints, faults, foliation, lineation, folds, and rock contacts. The primary access points to groundwater in basement rock include fissures and joints, as well as the intergranular pores found in the depositional regions of fine to coarse sands and gravels (Shuaibu, 2023).

Methodology

The study used two different geophysical instruments to conduct three geophysical techniques: Vertical Electrical Sounding (VES), Electrical Resistivity Tomography (ERT), and the Natural Electric Field method (NEF). Using an ABEM SAS-4000 Resistivity meter and a PQWT-TC150 Water-Detector equipment, respectively, Electrical Resistivity Tomography and the Natural Electric Field technique were employed during the reconnaissance survey phase. The ABEM Ohmega resistivity meter was then used for additional probing using Vertical Electrical Sounding (VES). The study area was divided into six profiles based on preliminary hydrogeological surveys and structural analysis of the area, ensuring coverage of all significant geological formations (Figure 3).

Electrical Resistivity Tomography (ERT)

ERT Data acquisition: This study made use of the Wenner array. Six (6) profiles were used for the measurements (Figure 3). Potential changes between electrodes were evaluated thoroughly and regulated current injections were used for ERT measurements. Six profiles were measured along a 240-meter line. There were 48 electrodes positioned every 5 meters along each profile. A clip was utilized to secure the smart electrode to the supplied multi-core cable, guaranteeing that there is

contact between them. The cable was placed in the ground and attached to electrodes. The Terameter automatically selected the active electrodes for each measurement, recorded a series of measurements, and simultaneously displayed the average results on its screen.

Moreover, the direct current (DC) was passed into the surface, and the voltage/current (V/I) ratio was automatically measured and recorded on the meter screen. After all, apparent resistivity (ρ_a) from the recorded potential differences was obtained as in equation (2).

$$\rho_m = \frac{1}{5f} \left(\frac{E_x}{H_y} \right)^2 \tag{1}$$

Where ρ_m represents the resistivity of the medium undergoing interaction, f denotes the operating frequency, and H_y and E_x denote the magnetic field and electric field components of the respective fields. Equation 2 serves to transform equation 1 into a one-dimensional depth inversion, assuming the 1D slice represents the earth with equal impedance.

$$\delta = 503.3 \sqrt{\frac{\rho}{f}} \tag{2}$$

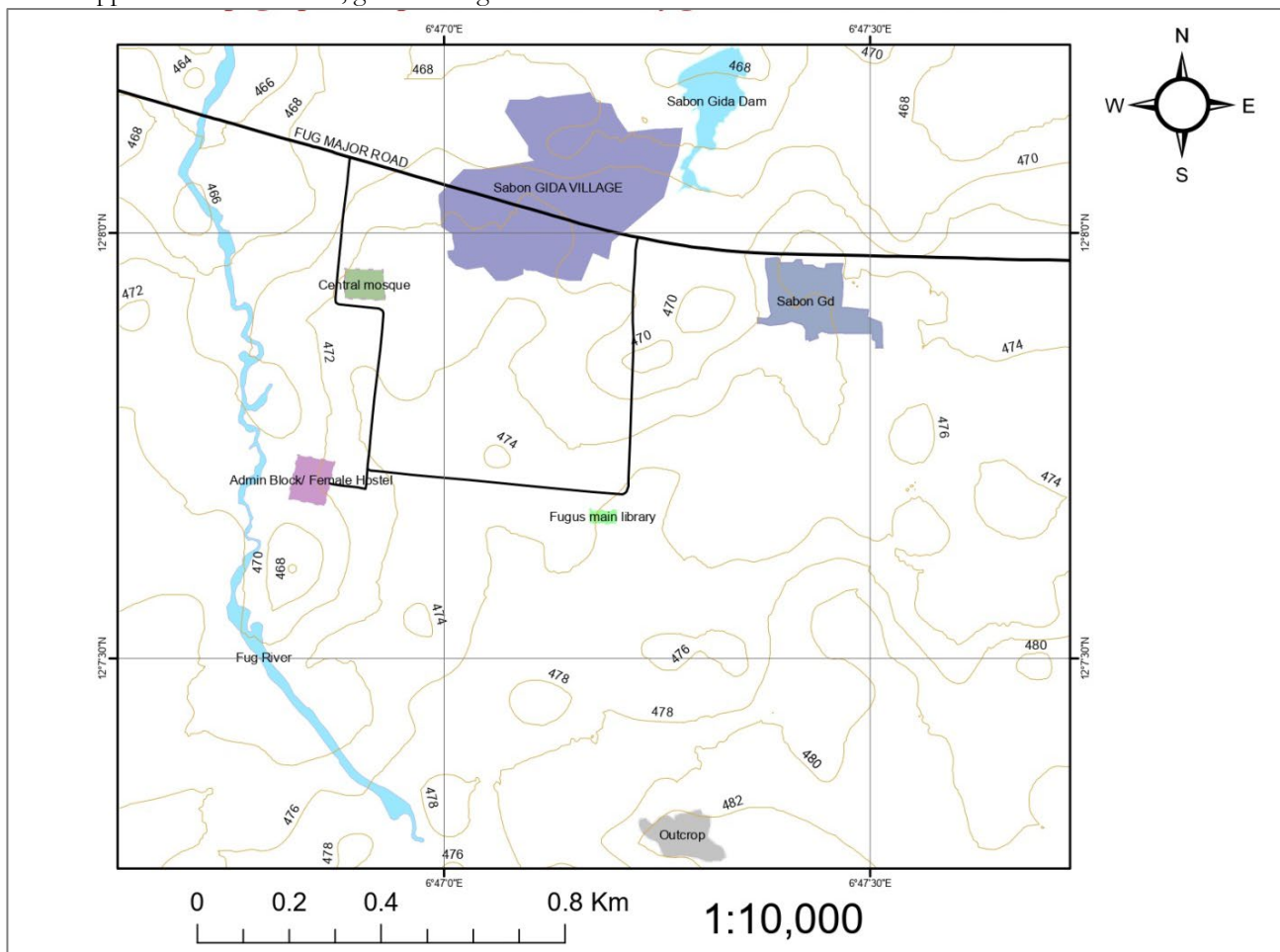


Figure 1: Topographic Map of the Area (Shuaibu, 2023)

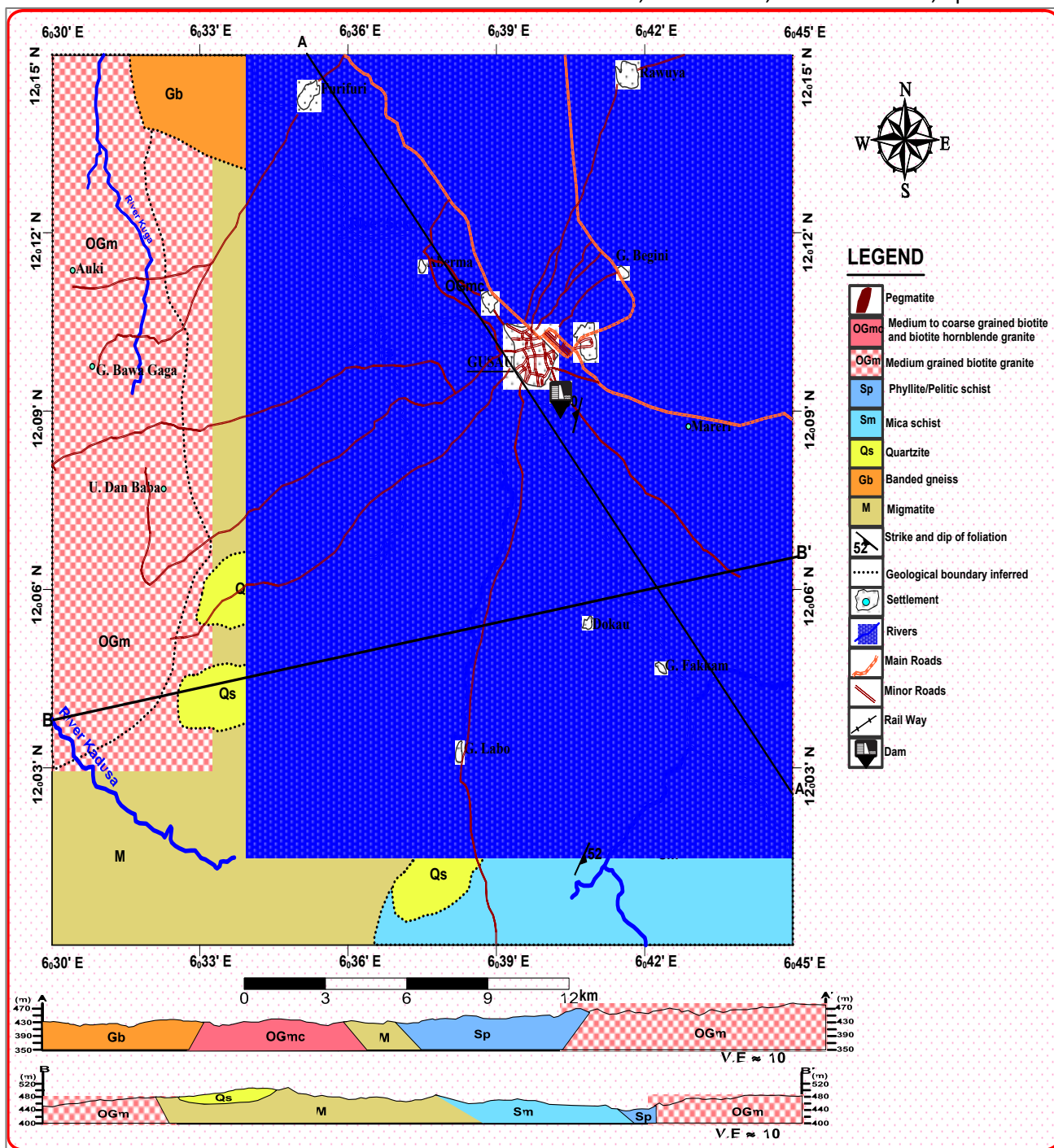


Figure 2: Geological Map of Gusau (Shuaibu, 2023)

A measured resistivity model was created using the data that was collected. Using the RES2DInv program, the measured apparent resistivity was inverted. A calculated resistivity model of the true resistivity was then generated using an inversion technique of robust or smoothness constraint. The inverted model (which displays an actual resistivity value that was compared to the geological resistivity table) was created by comparing the accuracy or resemblance of these two models. Additionally, resistivity contour, 2D, and 3D maps of the research region were created using SURFER 12 software.

Natural Electric Field Method

The PQTW-TC150 Water detector is a novel geophysical exploration tool that was used to measure the natural electric field in the EM Method. Because it uses the natural electric field as the field source, the device is also known as a natural electric field frequency selection system (Devi et al., 2001). The PQTW-TC150 model functions by utilizing variations in the conductivity characteristics of the underlying geological formations. It gauges the natural earth's magnetic field's electrical diversity as well as variations at various frequencies and depths (Figure 4).

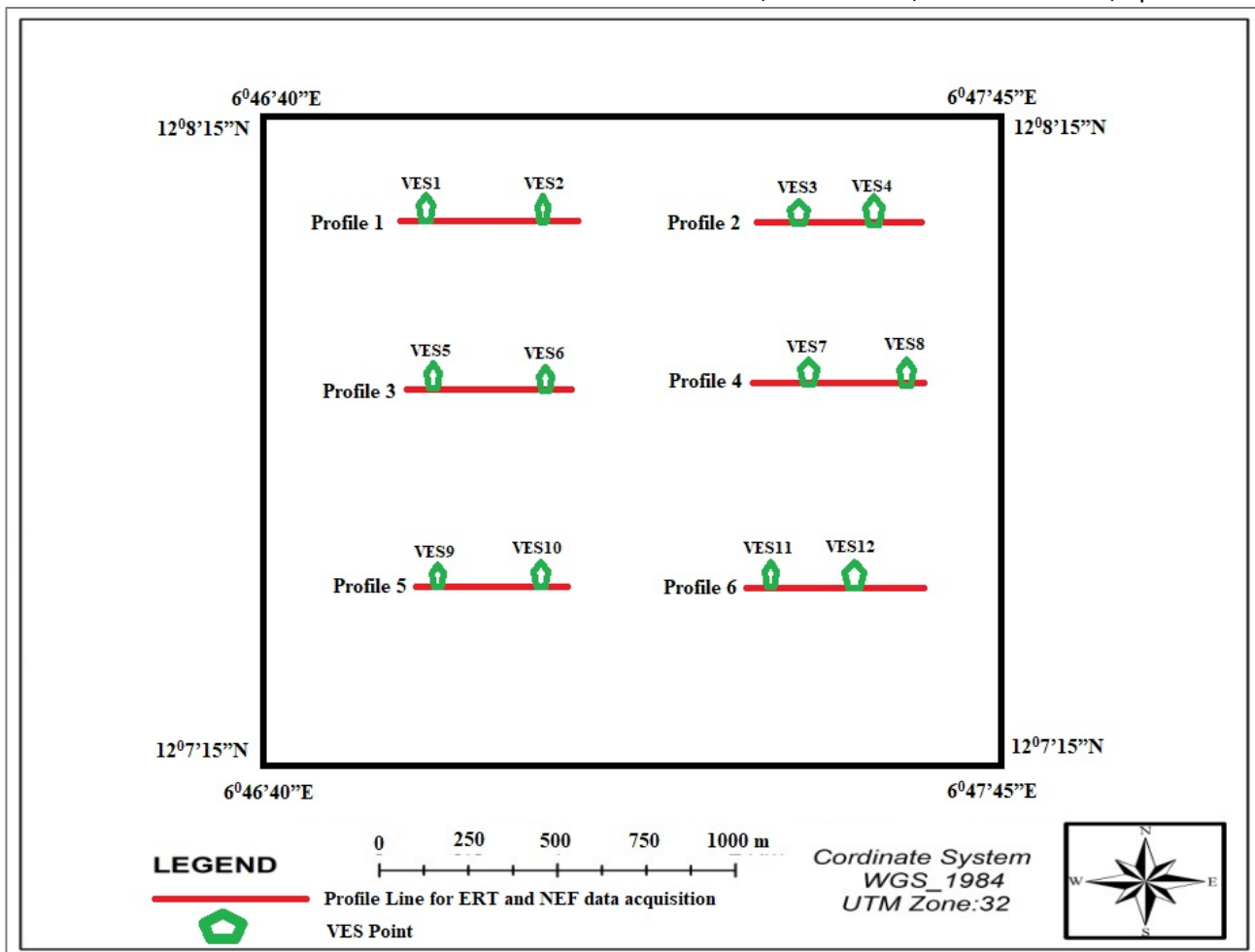


Figure 3: Map of Profile Lines

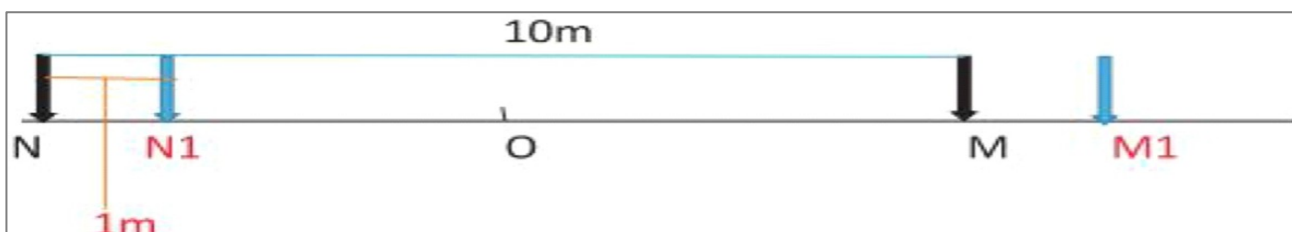


Figure 4: PQWT Instruments setup and electrode arrangement

In accordance with the ERT approach, six NEF method traverses were completed. To capture the initial reading on each traverse, the two potential electrodes were placed on the ground at positions N and M, 10 m apart, in order to do the field measurement. The probes were connected to the instrument using a console connection, which measures the electromagnetic impulse produced by those places and automatically saves the data. As a result, to obtain the next reading, the N and M electrodes were moved 5 m apart on the traverse line; that is, N was moved to 5 m and M to 15 m (Figure 4). Thus, these procedures were continued until the transversal was finished as a whole. The major data collected at the 21 distinct stations on each of the eight traverses in the research region are the electrical potential changes between the pairs of electrodes that make contact with the ground. With a single button press, the device calculates the electric field

component of 36 distinct frequencies in the geomagnetic field in millivolts (mV). The PQWT-TC150's display then generates a frequency curve along with a profile map. The frequency curve showed how the subsurface's typical frequency lines react when the device applies a little millivolt-level potential differential (Anbazhagan & Jothibas, 2016). A curving or angular frequency line indicates changes in the characteristics of the rock, whereas a straight line demonstrates a homogenous subsurface material. Using equations 1 and 2, the PQWT-TC150 algorithm generates a profile map using the electric field response in millivolts. Typically, a resistance bar is displayed on the right side of the map, ranging from red at the top to blue at the base (Ahmed et al., 2021). The red color scheme shows the highly resistive zones and the resistance decreases as the color spectrum moves towards the blue color. On the profile map, areas with a higher

propensity for groundwater are shown by a concentration of bluer color, and cracks and faults are visible where typical contour lines concentrate (Amadi *et al.*, 2011; Taweelarp *et al.*, 2021; Puttiwongrak *et al.*, 2022).

Using the PQWT-TC150, measurements of the natural electric field were made on each of the six traverses at intervals of 5 meters. The resulting frequency curve is a graph plotting the lateral sampling distance on the horizontal axis and the frequency responses of the earth's electromagnetic field in millivolts (mV) on the vertical axis. The accompanying profile maps give the visual (Subsurface Image in 2D) interpretation of the subsurface's frequency response down to 150 meters. The horizontal axis indicates the lateral distance traveled throughout the survey, while the vertical axis displays the depth into the subsurface. The contour lines on the profile map are mapped using the frequency response (numerical values), and the areas where the lines concentrate or diverge indicate the presence of significant anomalies.

Vertical Electrical Sounding

A total of twelve (12) Vertical Electrical Sounding (VES) points were conducted within the study area using ABEM Ohmega resistivity meter, to measure and record the resistance of the subsurface by Schlumberger configuration.

The VES stations were systematically selected at different locations based on the major rock/dominant structural trends within the study area. The potential electrodes remain fixed and the current electrodes were expanded simultaneously about the center of the spread. The maximum electrode separation used was $AB/2 = 100$ m and a maximum potential electrode spacing $MN/2 = 0.5$ m which are normally arranged in a straight line, with the potential electrode placed in between the current electrodes. This configuration is mostly used as it would provide sub-surface information considering the depth of penetration. The field data were converted to apparent resistivity (ρ) in ohm-meter by multiplying with Schlumberger geometric factor (K). Data interpretation was done through the help of computer software and basic geophysical principles based on geological structures. Software like IP2WIN was used.

The curves obtained were then compared to the H, K, Q, and A curve types. The distribution of resistivities of different subsurface layers is described as follows: H-type, $\rho_1 > \rho_2 < \rho_3$; K-type, $\rho_1 < \rho_2 > \rho_3$; A-type, $\rho_1 < \rho_2 < \rho_3$; Q-type, $\rho_1 > \rho_2 > \rho_3$; KA, HQ-type, and so on, represents four curve layers.

RESULTS AND DISCUSSION

Electrical Resistivity Imaging (ERT Method)

Profile 1 of ERT was run in the NW-SE direction, and the modelled section indicates continuous lateral and vertical inhomogeneous beds, as shown in Figure 5. The ERT

result revealed the presence of three major geoelectrical layers having a wide range in the apparent resistivity reading between $21\Omega\text{m}$ and $931\Omega\text{m}$ across two to three zones. The first zone consists of resistivity values ranging from $21\Omega\text{m}$ and $183\Omega\text{m}$; the second zone has resistivity of $21\Omega\text{m}$ to $62.1\Omega\text{m}$, while the third zone's resistivity is between $187\Omega\text{m}$ to $931\Omega\text{m}$.

The resistivity of the top layer (Overburden) can be placed into two groups: the first group has low resistivity ($21 - 62.1\Omega\text{m}$) and is mainly clayey to silty sediments with thickness between 1 and 5m. This zone is dominant, especially from 0-32m at a horizontal distance, and starts again from 60m to the end of the profile at a lateral distance along the profile. The second group has high resistivity ($62.1 - 183\Omega\text{m}$), which represents indurated sediments with the presence of ferruginized claystone nodules. This part of the layer is present at 33-60m horizontally along the profile and also has a thickness of 1-5m. The second layer, which forms the weathered/fractured basement (aquiferous zone), has a low resistivity of ($21 - 62.1\Omega\text{m}$) and a thickness of 19-23m across the entire study area. The third geoelectrical layer has a resistivity value ranging from $187-931\Omega\text{m}$, forms an un-fractured zone (fresh basement/ non-aquiferous zone).

Suitable points such as the 40 and 96 m lateral distance along the traverse were selected for VES1 and 2.

Profile 2 was also run in the E-W direction; the resistivity sections of Profile 2 consist of three layers, as shown in Figure 6. The first layer has an apparent resistivity of 21.3 to $28.1\Omega\text{m}$, which consists of sandy-clays to a shallow depth of 4m. The second layer is a high to intermediate resistive layer with a resistivity range of $37\Omega\text{m}$ to $112\Omega\text{m}$, which is interpreted as weathered basement. This layer is present from depth of 4 - 12 meters around 0 - 65 lateral distance and to infinity at 65-120m lateral distance. The third layer is interpreted as a fractured basement layer, with saturation increasing with depth. The third layer is made up fractured aquifers with a lower resistivity range in comparison to the other two layers, which also reflects its possible high saturation. It has an apparent resistivity range of $16.2\Omega\text{m}$ and $37.8\Omega\text{m}$, with least values obtained around center of the profile. This layer occurs from about 12 meters at a lateral distance of 0 - 65m horizontally along the profile. The deeper layer of fresh basement is absent in this profile.

The 2D resistivity section obtained from the inversion of profile 3 is displayed in Figure 7. The image shows three (3) geoelectric zones beneath the profile. These include the overburden, which can be placed into two groups: the first group has low resistivity of ($6.36 - 46.3\Omega\text{m}$) and is mainly clayey to silty sediments with thickness between 1 - 12.4m. This zone is dominant, especially from 0 - 110m at lateral distance along the profile. The second group of the first layer has high and medium resistivity ($126 - 6889\Omega\text{m}$), which represents indurated sediments with the presence of compacted laterite. This part of the layer is present at 110m to the end of the profile horizontally

along the profile from the top to the depth of 12.4m, with resistivity ranging from 126 ohm-m to 6889 ohm-m. The second subsurface geoelectric layer has a very high resistivity value compared to other geo-electrical layers ranging from about 6.36 ohm-m to about 126 ohm-m, its interpreted as highly fracture zone forming aquifers and has thickness of about 12 - 28.7m. The third geoelectric layer has medium resistivity of about 126-344ohms and extends from a depth of 28.7m, the layer is interpreted as basement with very slight fractures.

Suitable points such as the 60 and 130m at lateral distance along the traverse were selected for VES5 and 6.

The inverted 2D resistivity image along traverse 4 (profile 4) is shown in Figure 8. The image shows the general resistivity distribution beneath the traverse with a prominent clayey-laterite layer at to the top to the depth of 6m and resistivity of (28.3 - 94.80 ohm-m). The second layer, with very low resistivity of (28.3 - 174 ohms-m) is interpreted to be a weathered/fractured zone and has a thickness of about 6 - 30m. This layer is suspected to be the aquifer where groundwater could be tapped. The third layer has of high resistivity value ranging from (174 – 1065 ohms-m) is interpreted as fresh-basement.

Suitable points such as the 80 and 120m at lateral distances along the traverse were selected for VES7 and 8.

The ERI profile 5 was run in the E-W direction, and the modelled-section indicates continuous lateral and vertical inhomogeneous beds, as shown in Figure 9. The resistivity of the top layer (Overburden) can be placed into two groups: the first group has medium resistivity (21 -

51.2Ωm) and is mainly sandy laterite with thickness between 1 and 5m. This zone is dominant, especially from the profile, starting from point 0 - 32m and then starting again from 110m to the end of the profile. The second group has high resistivity (124 - 382Ωm), which represents indurated highly compacted sandy-laterite. This part of the layer is present at 40 - 110m horizontally along the profile and also has a thickness of 1 - 5m. The second layer has slightly less resistivity values compare to the other layer (21 – 51.2Ωm) and thickness of 6 - 28m across the entire study area. This layer is interpreted as a weathered/slightly fractured basement (partially aquiferous zone). The third geoelectrical layer, with a high resistivity value 124 - 731, forming un-fractured zone (fresh basement/non-aquiferous zone). This part of the study has low-medium groundwater potential compare to the other part.

Suitable points such as the 60 and 100 m lateral distance along the traverse were selected for VES 9 and 10.

Profile 6 was also run in the E-W direction; the resistivity sections of the profile consist of three layers, as shown in Figure 10. The first layer has low apparent resistivity of 16.7 to 51.8Ωm, which consists of sandy-clays to a depth of 13m. The second layer has a resistivity of 51.8 - 156 Ωm, with thickness of 13 - 29m. This layer is interpreted as weathered/partially fractured basement, and the yield at this zone was predicted as low-moderate. The third geoelectric layer is made up of fresh basement with high resistivity value ranging from 272 - 823 Ωm, at the depth of 29m.

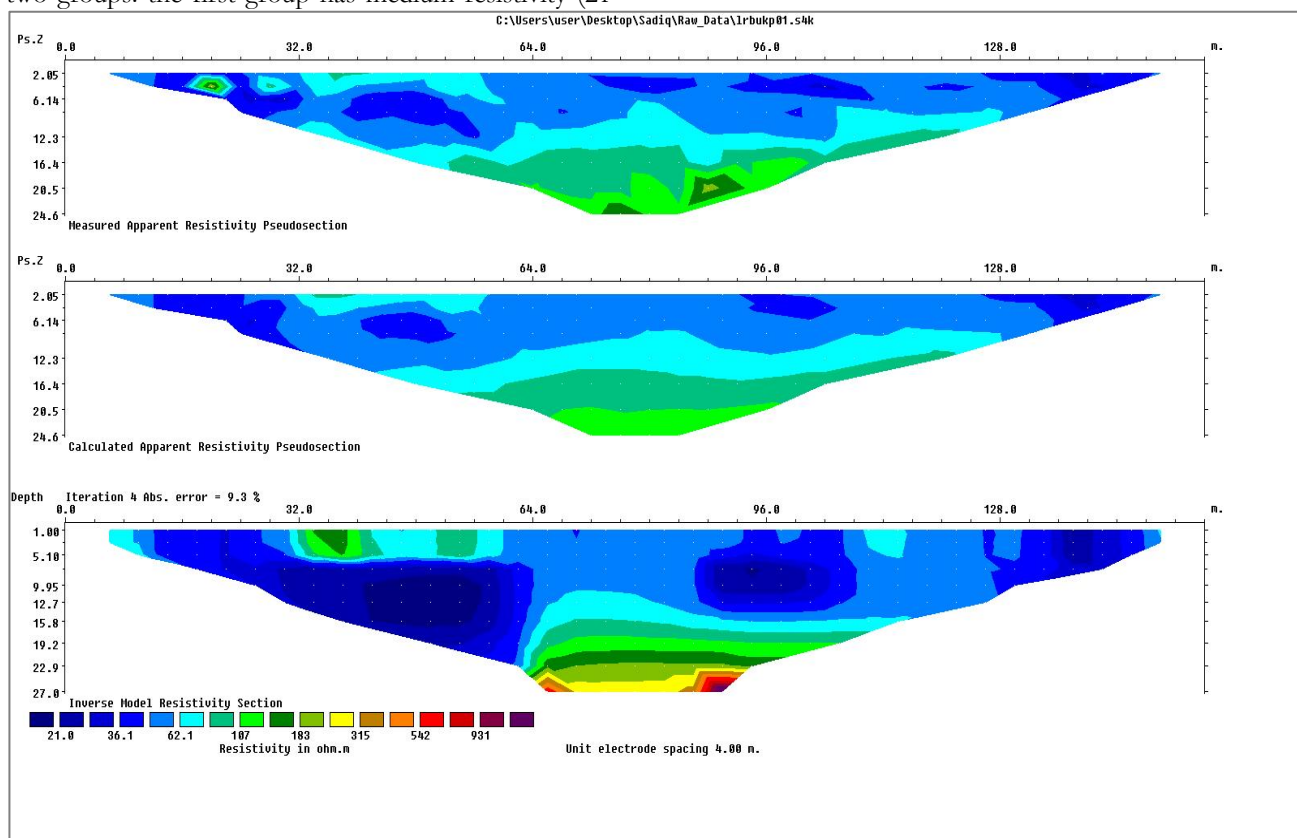


Figure 5: 2D Resistivity Section along Traverse 1

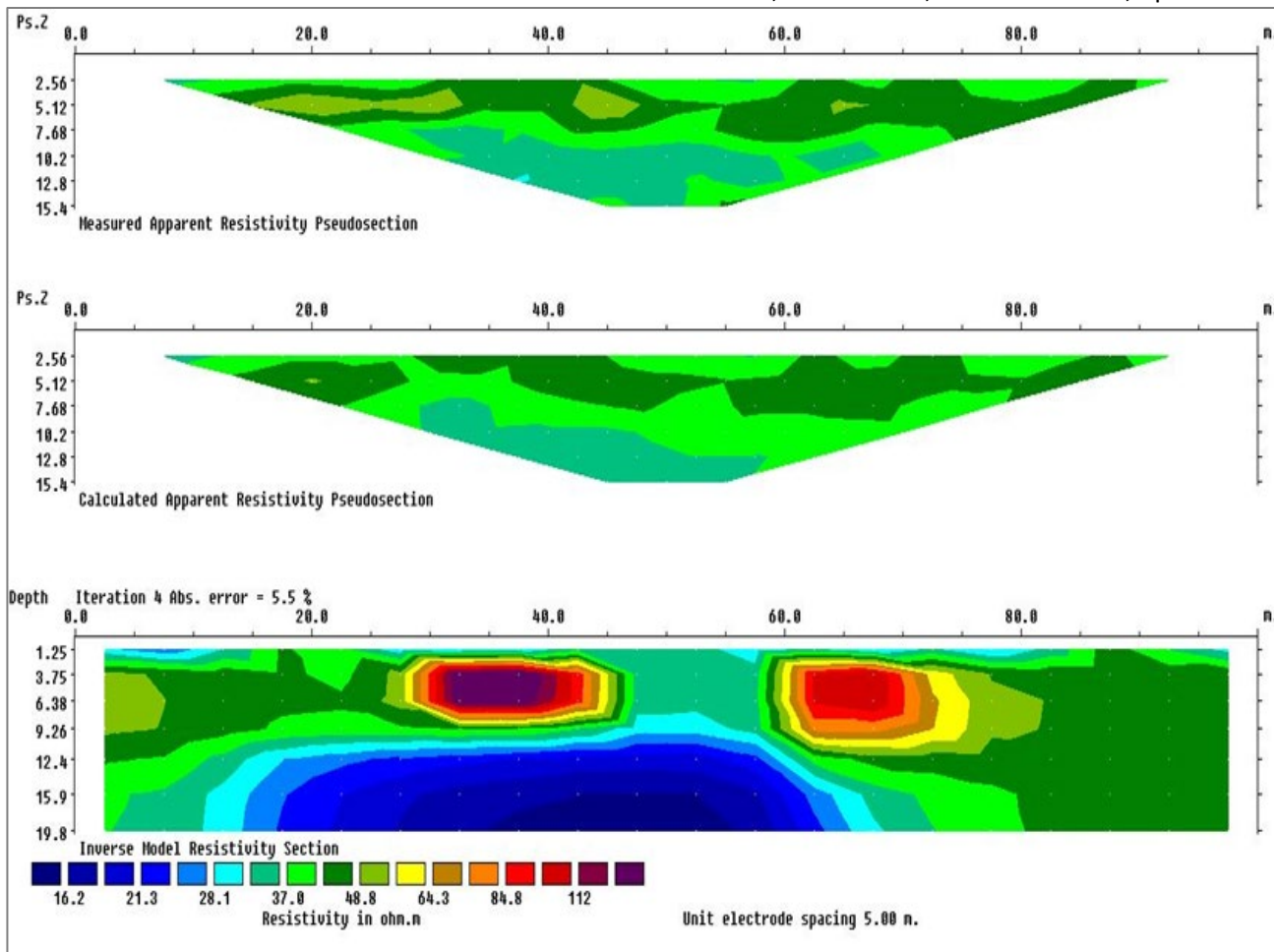


Figure 6: 2D Resistivity Section along Traverse 2

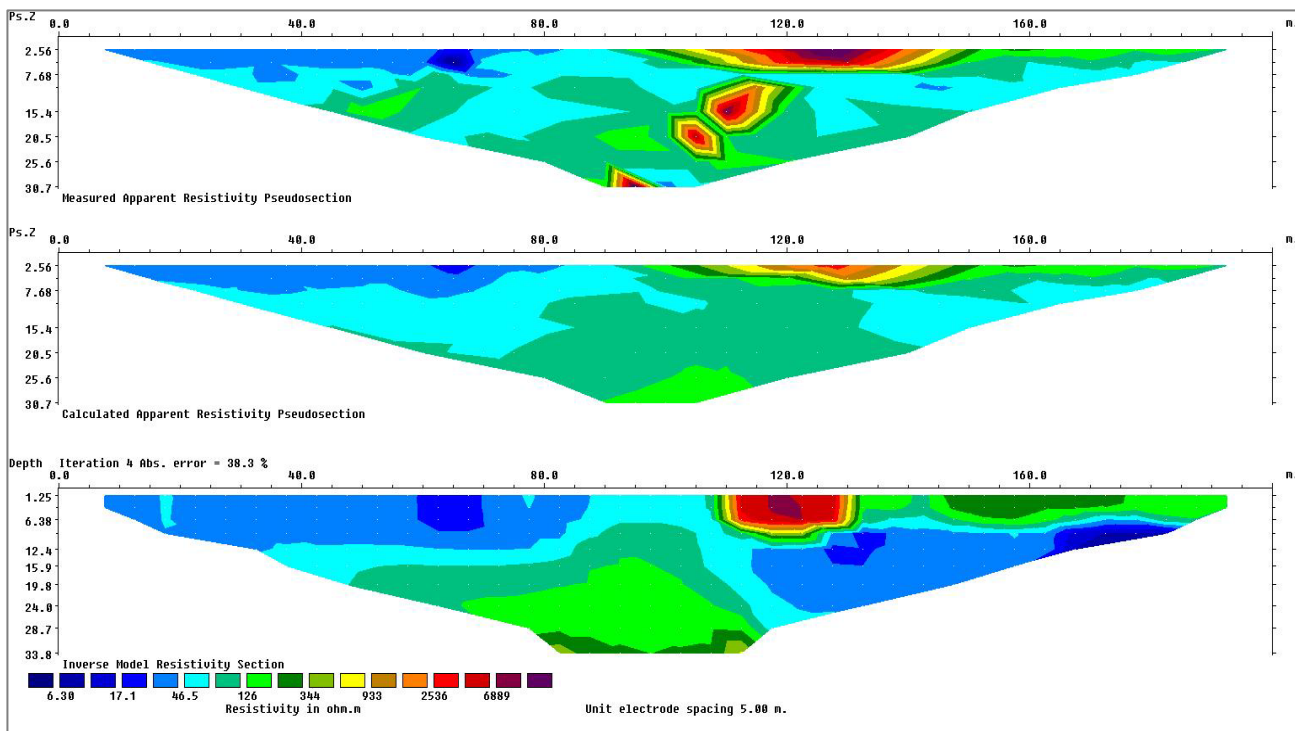


Figure 7: 2D Resistivity Section along Traverse 3

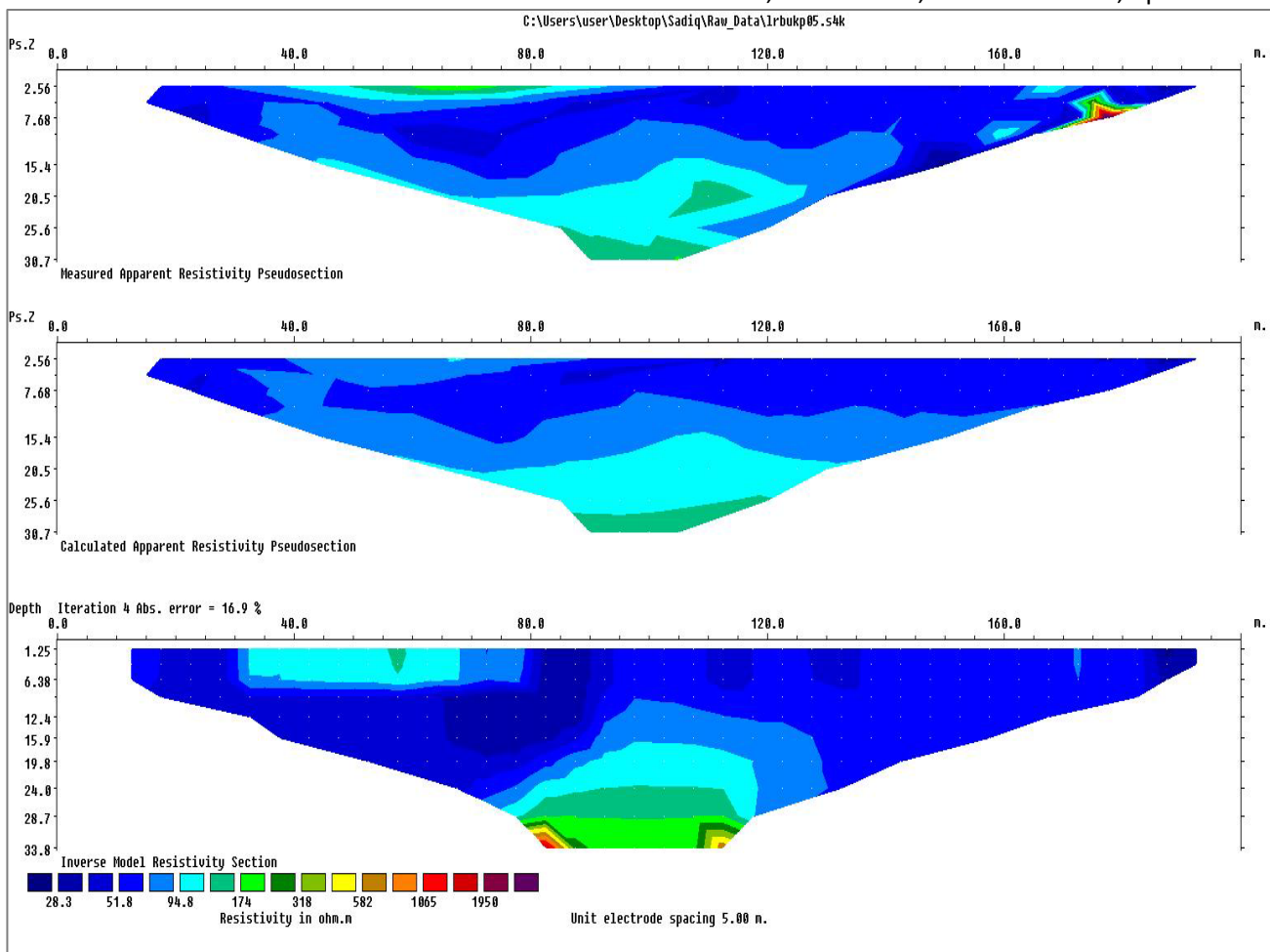


Figure 8: 2D Resistivity Section along Traverse 4

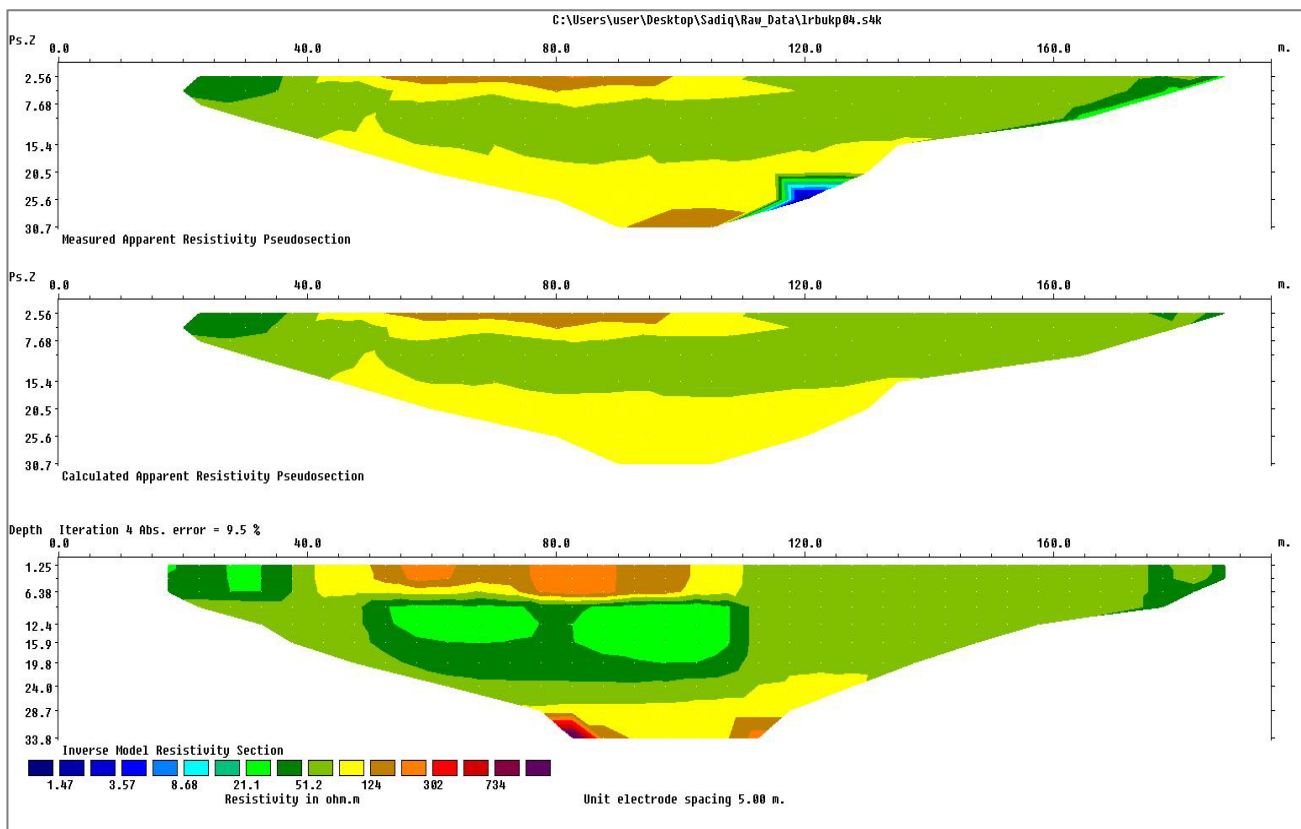


Figure 9: 2D Resistivity Section along Traverse 5

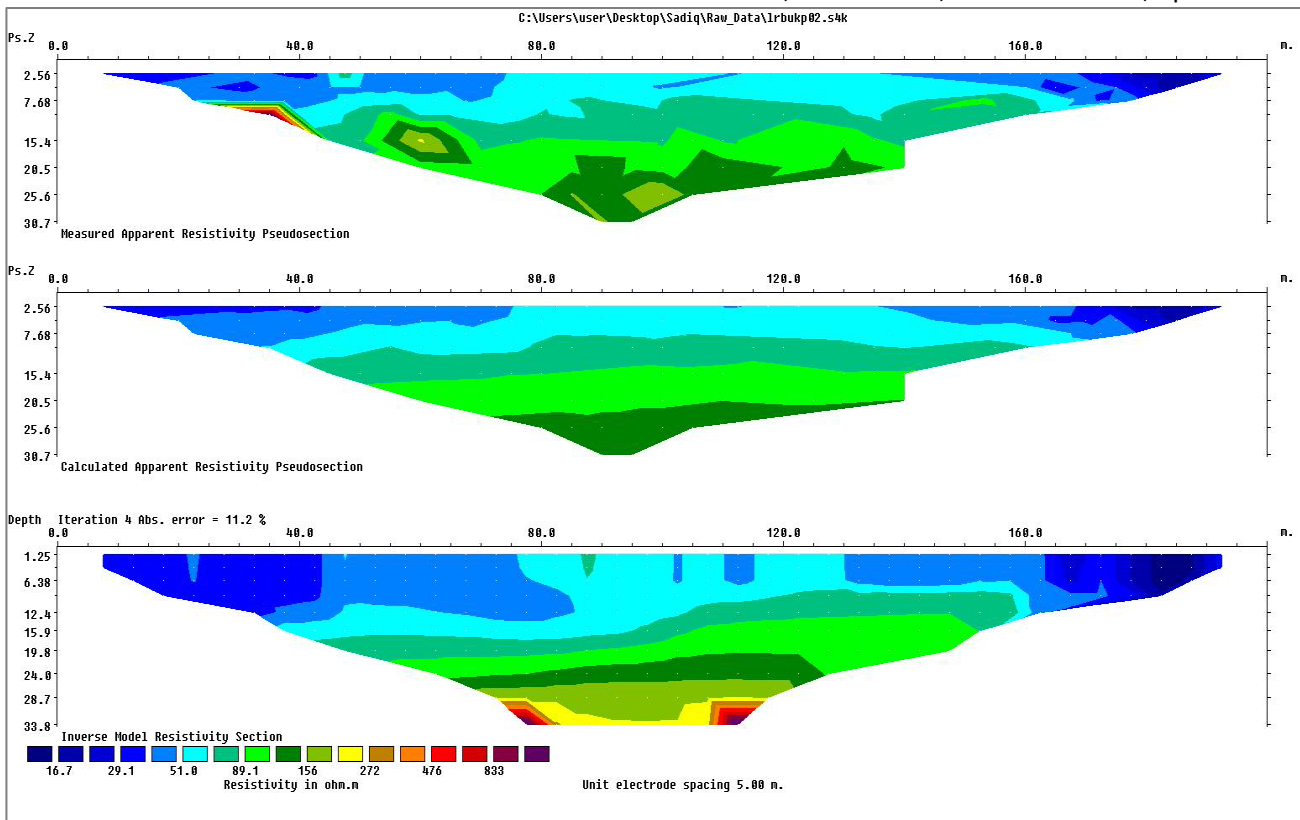


Figure 10: 2D Resistivity Section along Traverse 6

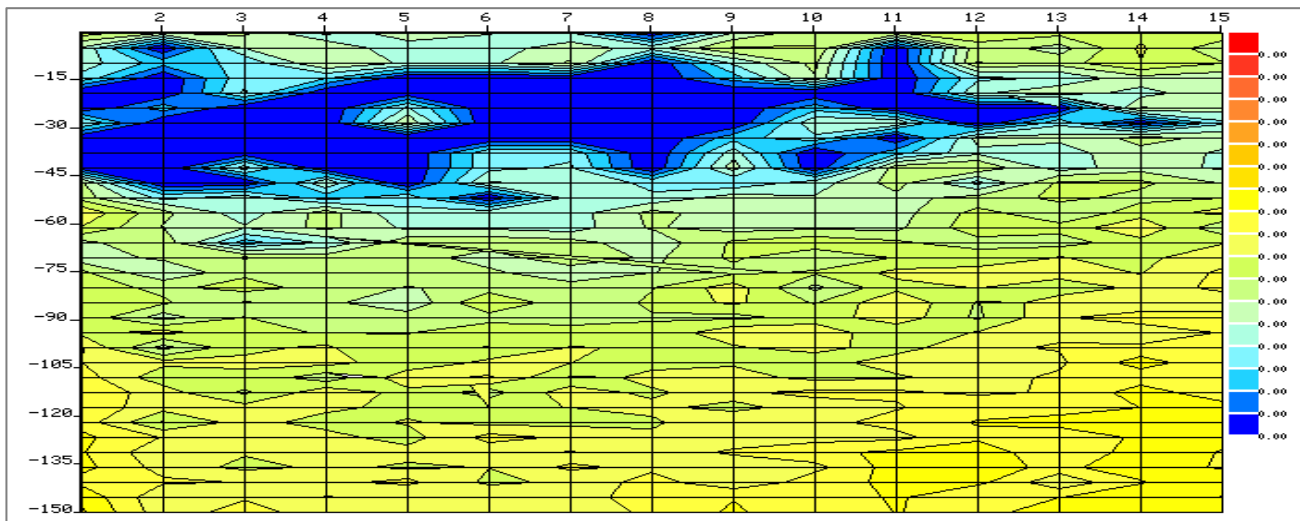


Figure 11: Frequency Curve Along Profile 1

Natural Electric Field Measurement (NEF Method)

At the first measurement (station 1), the frequency curve from traverse 1 shows a peak potential response of 2.1 mV. Interestingly, for the whole profile length and at stations 3–6, normal frequency lines show characteristic curved responses (Figure 11). These curved responses on the profile map are understood as concentrated fractures at stations 6 to 10 (15 to 50m) and horizontal fractures between stations 3 to 6 (50 to 65m). Overburden, or loose rock elements, makes up the top layer of this traverse and extends down to roughly 10 m. Below that is a lower resistive layer that descends to around 90 m. After 90 meters, the subsurface exhibits a moderate resistance

characteristic with different contour line concentrations (Figure 11).

The frequency curve in the second traverse (profile 2) shows a peak potential response of 2.0 mV at profile station 1 (Figure 12). At stations 6 and 7, the potential response then drops to around 0.0–0.1 mV. This is seen on the profile map as a severely fragmented zone with extremely low resistance at depths between 45 and 150 m. Furthermore, there is another noticeable drop at stations 2–4, which is depicted on the profile map as a vertical fracture at a depth of 45–100 meters. This traverse's top layer is somewhat resistant down to an average depth of 45 meters below the surface, much like the treks that came

before it. Moreover, a very resistant substance is found at a depth of more than 120 meters from the surface.

On third profile, station 18 experiences a peak potential response of 3.7 mV, and at station 13, there are further sharp swings that decrease to 0.0 mV (Figure 13). Based on the profile map, these responses are interpreted as a vertical fracture that extends from 90 to 110 meters below the surface and is centered at station 13. An additional

steep decline is noted at stations 14 and 15, which the profile map interprets as several vertical cracks extending from the surface to a depth of 50 meters. This traverse's top layer is found to be low resistive up to an average depth of 70 meters below the surface, much like the previous traverses. Moreover, a highly resistant body is found more than 120 meters below the surface of the ground.

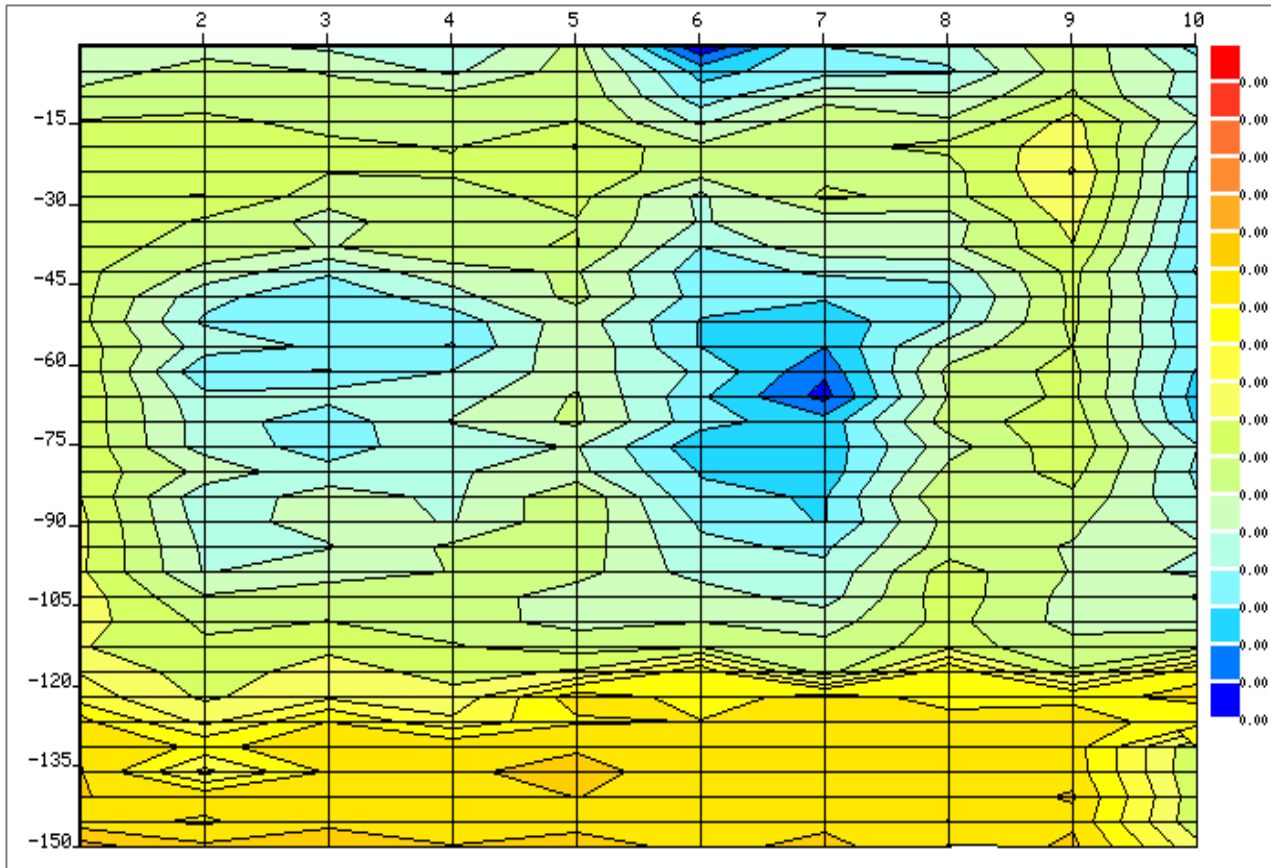


Figure 12: Frequency Curve Along Profile 2

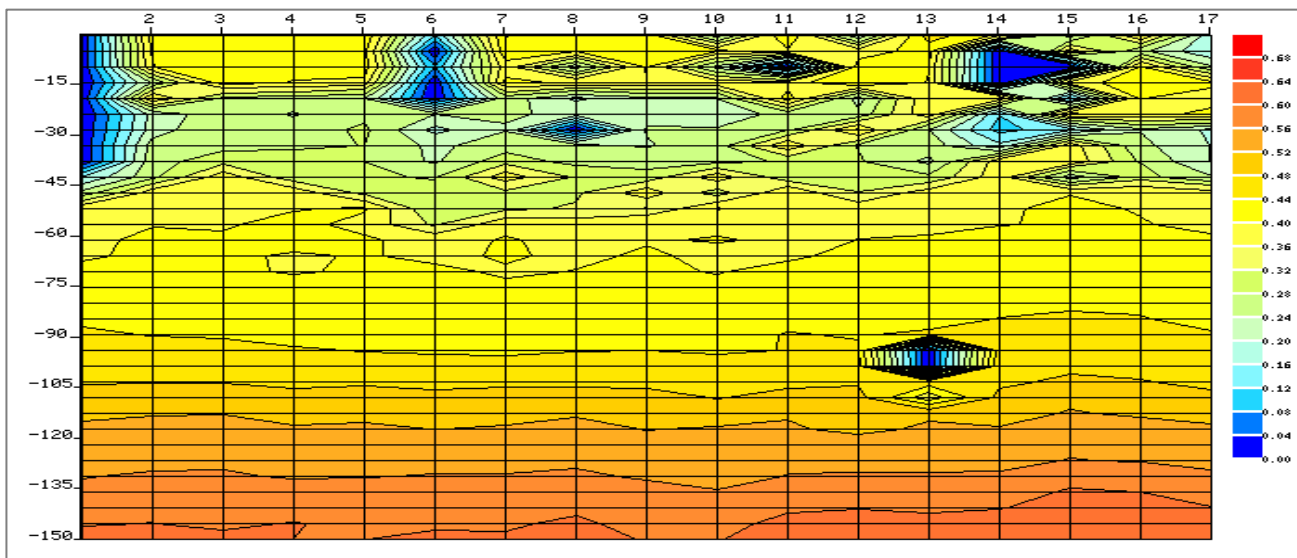


Figure 13: Frequency Curve of Profile 3

The frequency curve displays a peak potential response of 3.30 mV at station 3 on the profile in the fourth traverse

(profile 4) (Figure 14). At shallow depths of between 10 and 30 meters, the potential response then drops to about

0.0 to 0.1 mV over most of the stations. This is depicted on the profile map as a heavily fragmented zone with very low resistance. The top layer of this trip is somewhat resistive up to an average depth of 5–10 meters below the

surface, much like the preceding travels. Moreover, at a depth of more than 40 meters below the surface of the ground, a very resistant mass is found (Figure 14).

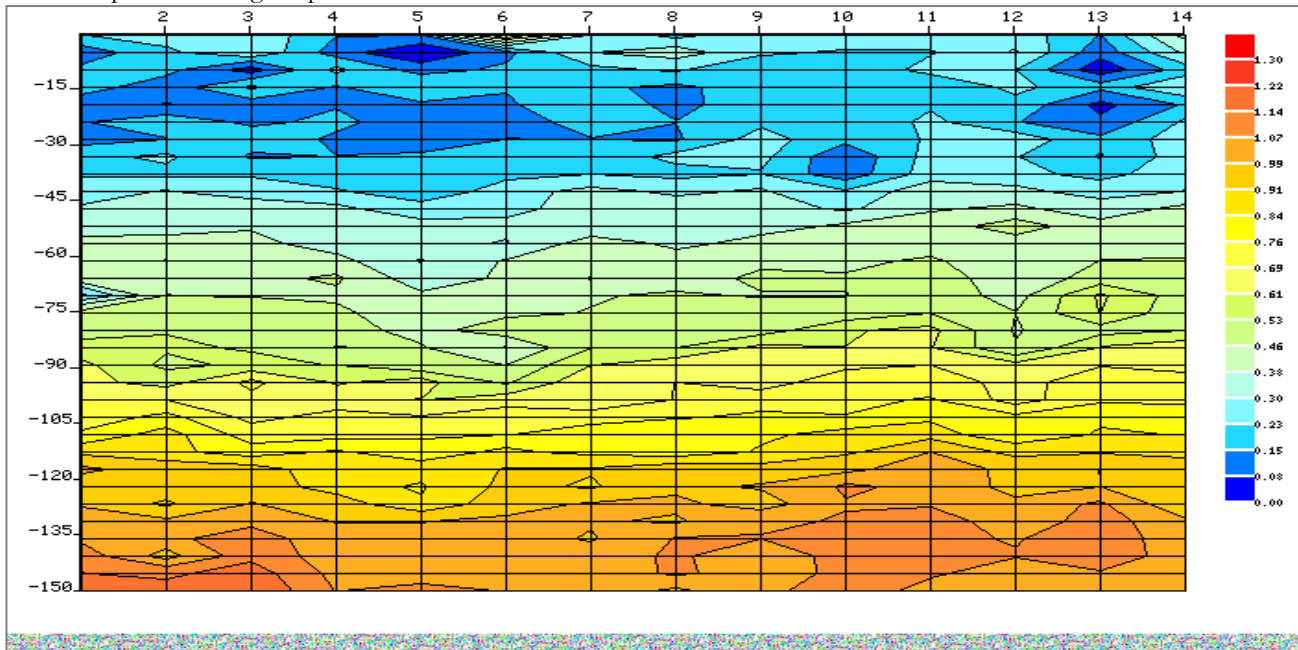


Figure 14: Frequency Curve of Profile 4

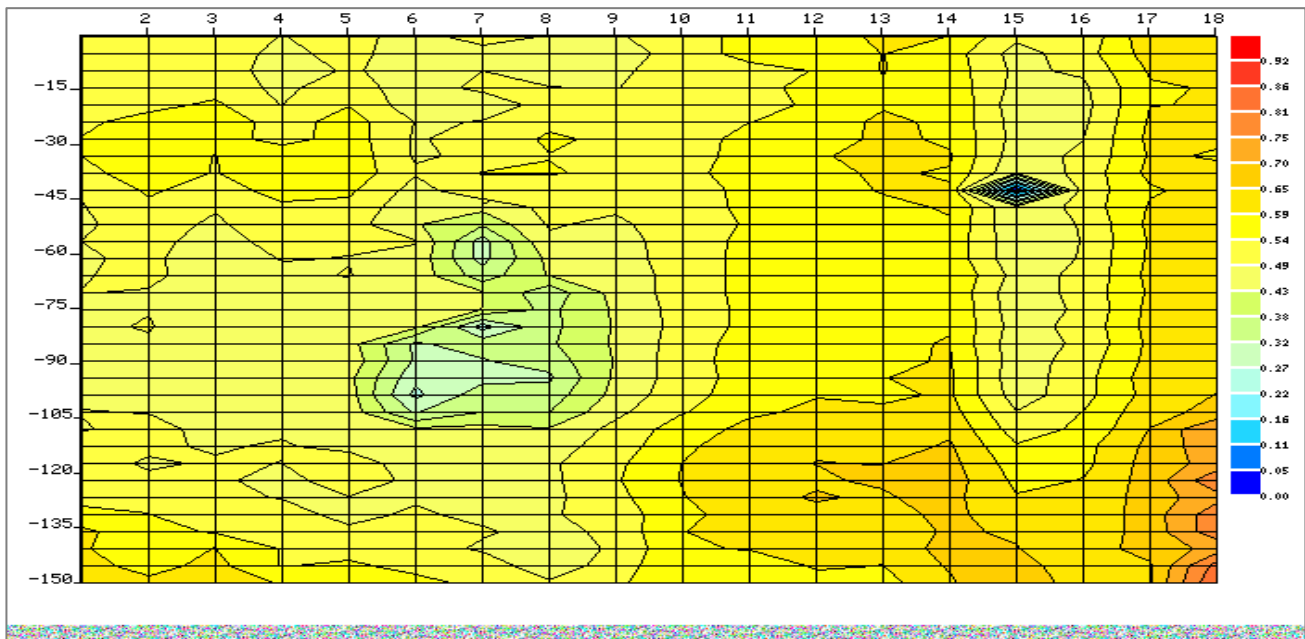


Figure 15: Frequency Curve of Profile 5

During the sixth traverse, stations 6 to 8 exhibit sharp variations ranging from 2.0 to 1.0 mV, whereas station 18 experiences a peak potential response of 3.4 mV (Figure 15). These responses, which occur between 50 and 110 meters below the surface of the earth, are interpreted on the profile map as a vertical fracture at stations 6 to 8 (110 meters). At station 15, there is another noticeable dip that is thought to be a precise vertical fracture that occurs at a depth of 45 meters. Up to an average depth of 45 meters below the surface, the upper layer of this traverse has a moderate resistance. Furthermore, at station 18, a highly

resistant body is found at a depth of more than 110 meters below the surface of the earth (Figure 15).

At stations 4, 5, and 12 in the six traverse (profile 6), there is a peak potential response of 1.0 mV. At a depth of 15 to 20 m, this response quickly drops to 0.0 mV (Figure 16). The profile map interprets these responses as a horizontal fracture that spans depths of 15 to 20 meters below the surface and is centered at stations 4, 5, and 12. Like the other traverses, this one's overburden layer is found to be low resistive down to an average depth of 10 m, after which it is weathered/fractured and very low

resistive down to a depth of 20 m from the surface. Moreover, a highly resistant body is found more than 60 meters below the surface of the ground.

Vertical Electrical Sounding (VES)

Using a Schlumberger array, an electrical resistivity investigation was carried out at the thick overburden and

high conductive/fracture zones identified along the ERT and NEF profile lines. Table 1 summarizes the interpreted layer characteristics for each VES station based on 1D-resistivity curves (Figure 17). On the other hand, the bedrock is made up of fractured and fresh basement rocks, whereas the top soil, lateritic soil, and weathered basement are considered the overburden.

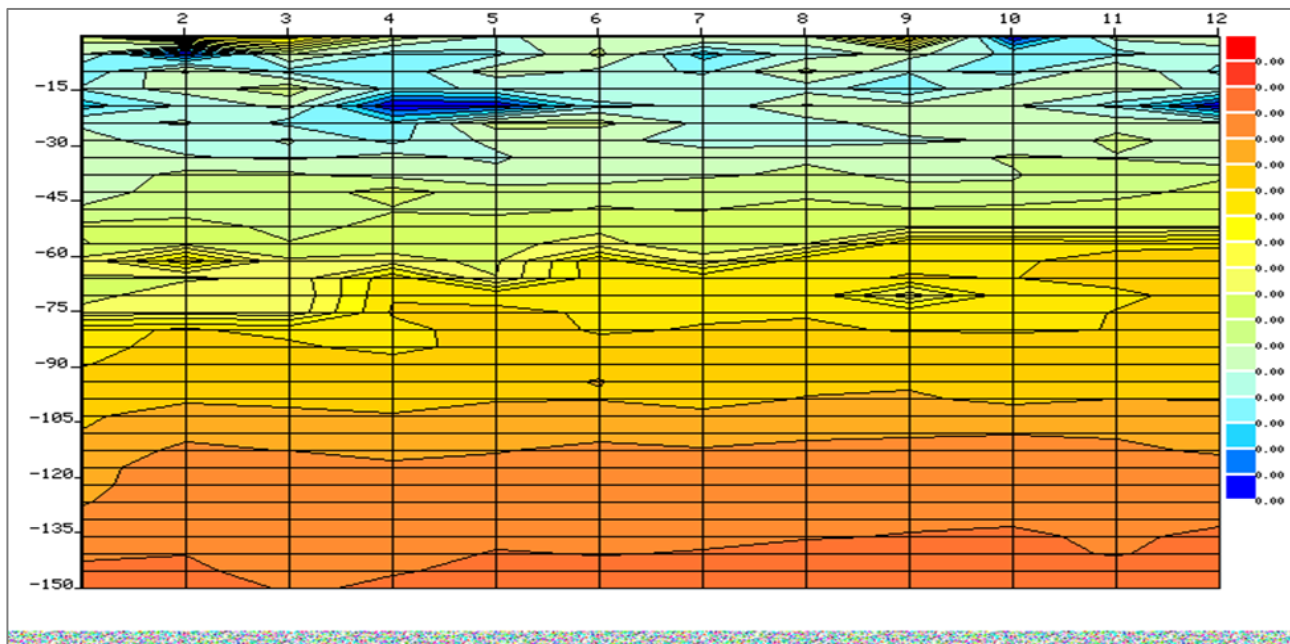


Figure 16: Frequency Curve of Profile 6

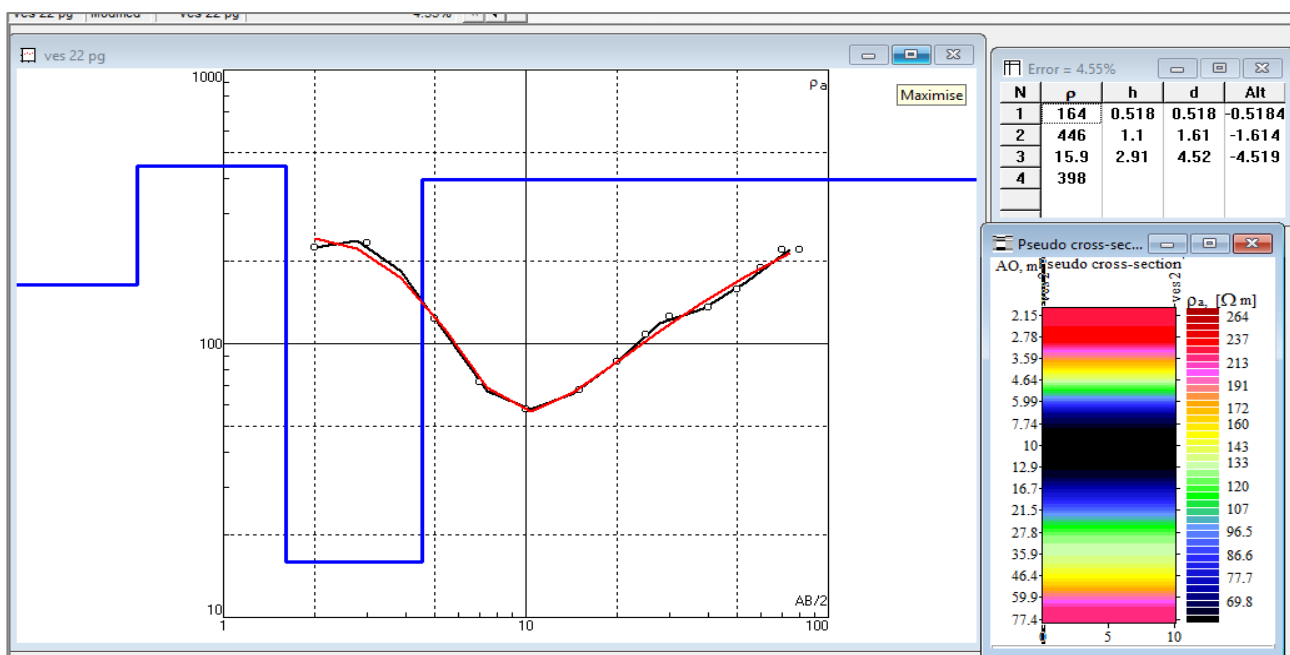


Figure 17: Selected Graph of Resistivity versus Current Electrode within the Study Area

The curve types observed in the area are of five types: KH-type (33%), H-type (25%), HK-type (25%), KA-type, and HA-type (17%).

The geoelectrical interpretation revealed 3 - 5 geo-electric layers: topsoil (10.8 - 356 Ωm), laterite soil/ clayey laterite (21.4 - 1402 Ωm), underneath it is a weathered basement

(9.9651 Ωm), underlying this layer is the fractured basement (21.7 - 859 Ωm) and the fresh basement (233 - 17272 Ωm). The thickness of overburdened material (comprising topsoil, lateritic sand, and clayey laterite) ranges from 3.14-10.2m. The next layer, which is the weathered basement, has a thickness range from 6.35-36. Underlying this layer is the fractured basement with

thickness ranging from 12.5-60m except in VES 3, 4, 6, 9, 11 where fractured layer reaches infinity (to depth of investigation), the last layer is fresh basement, even though

there's absent of fresh basement layer in some VES point. The fracture layer thickness in both the VES is good enough for groundwater potential.

Table 1: Interpreted Geo-electrical Layered Parameter of the Study area

VES No.	Layers/Curve Type	Resistivity (Ω m)	Thickness (m)	Depth (m)	Layer Characteristics
VES 1	KH	130	1.12	1.12	Topsoil
		1402	3.15	4.27	Compacted Laterite
		79.8	20	24.3	weathered basement
		594	36.1	60.4	fractured basement
		17272			Fresh Basement
VES 2	H	90.6	1.02	1.02	Topsoil
		665	4.83	5.86	Lateritic soil
		63.7	16.5	22.3	weathered basement
		598	33.4	55.7	Fractured Basement
		3151			Fresh Basement
VES 3	H	63.7	6.96	6.96	Topsoil/Literite
		24.6	29.1	36	weathered/slightly fractured basement
		284			Fractured Basement
VES 4	KH	71.7	1.34	1.34	Topsoil
		25.1	4.26	5.6	Lateritic soil
		13.4	4.56	10.2	Clayey laterite
		5134	17.9	28	Weathered basement
		56.5			Fractured basement
VES 5	KH	248	1.0	1.0	clayey topsoil
		577	6.34	7.34	lateritic soil
		72.3	13.8	21.1	weathered basement
		222	29.4	50.5	fractured basement
		4481			fresh basement
VES 6	H	267	0.872	0.872	Topsoil
		37.3	5.83	6.7	lateritic topsoil
		2139	5.79	12.5	weathered basement
		108			fractured basement
VES 7	HA	84.8	1.38	1.38	topsoil
		10.8	6.35	6.35	weathered basement
		108	17.3	25.05	fractured basement
		1110			fresh basement
VES 8	HK	21	2.77	2.77	Clayey Laterite
		9.29	2.715	5.48	weathered basement
		21.7	13.6	25.2	fractured basement
		5481			fresh basement
VES 9	HK	51.9	0.938	0.938	top soil
		317	0.645	1.58	lateritic soil
		22.6	5.65	7.24	clayey soil
		9651	10.57	17.81	weathered basement
		859			fractured basement
VES 10	KH	3787	2.13	2.13	compacted lateritic soil
		36.8	8.82	8.82	clayey laterite
		263	5.19	16.1	weathered basement
		312	30.3	46.4	fractured basement
		7282			fresh basement
VES 11	HK	57.7	3.74	3.74	Lateritic Top soul
		9.85	3.14	6.88	Clayey laterite
		1741	8.46	15.3	weathered basement
		891	24.5	39.8	highly fractured basement
VES 12	KA	12.8	3.82	3.82	Laterite
		72	8.15	12	weathered Basement
		25.6	8.56	20.5	highly fractured basement
		233			Fresh Basement

Due to the wider coverage of electrode spreading using the wenner configuration for ERT, the result revealed lithological information at greater depth in comparison with vertical electrical sounding. The 2D image equally provided an easy and clearer interpretation of the subsurface groundwater potential of the study area.

The NEF method proved particularly effective in identifying deep aquiferous zones, offering greater depth coverage compared to ERT and VES, which were more useful in mapping shallow fractures.

Integrating the results of the three techniques, it is clear that only weathered and fractured layers can serve as aquiferous units at a plausible depth of 60m across the study area. However, the fracture layer was identified as the most prolific zone for groundwater development.

The identification of fractured and weathered basement layers as aquiferous zones is consistent with previous studies in basement complexes across Africa (Ojo *et al.*, 2015; Marere *et al.*, 2023), highlighting the importance of geophysical techniques in addressing water scarcity.

CONCLUSION

The ERT method delineated two to three geoelectrical resistivity layers, including topsoil/laterite (overburden), weathered/fractured basement (aquifer), and fresh/slightly fractured basement. The interpreted results from the six profiles suggest groundwater development at an average depth of 60m within the fractured layer of the basement rocks.

The NEF method identified topsoil/laterite and weathered/fractured aquifer units, with significant aquiferous zones detected at various depths up to 150m. VES data corroborated these findings, revealing 3-5 geoelectrical layers, including topsoil, laterite soil/clayey laterite, weathered basement, fractured basement, and fresh basement.

The study concluded that both ERT and NEF methods are effective in identifying groundwater potential zones, with NEF offering the advantage of direct 2D subsurface visualization and greater depth coverage. The integration of these techniques demonstrated that NEF instruments provide comparable accuracy to conventional resistivity meters. The findings indicate significant groundwater potential in the study area, with well-developed fractured zones in the ERT profiles and substantial aquiferous zones in the NEF traverses, validated by VES data.

Overall, this research confirms the reliability of ERT and NEF methods for groundwater investigation in the Nigerian Basement Complex, highlighting the NEF method as a superior tool for hydrogeophysical exploration due to its depth coverage and ease of use. Future studies should explore the NEF method's application in different geological settings to further establish its efficacy in groundwater exploration.

The results suggest that future groundwater exploration efforts should focus on the weathered and fractured basement zones, particularly at depths of 20–80 meters. Further studies should explore the integration of additional geophysical techniques (seismic survey) to enhance the accuracy of subsurface mapping.

REFERENCES

- Agbasi, O.E.; Edet, S.E. Hydro-Geoelectric Study of Aquifer Potential in Parts of Ikot Abasi Local Government Area, Akwa Ibom State Using Electrical Sensitivity Soundings. *Int. J. Geol. Earth Sci.* 2016, 2, 1–15. [researchgate.net](https://doi.org/10.21961/ijges.v2i1.1).
- Ahmed, A.; Alrajhi, A.; Alquwaizany, A.S. Identification of Groundwater Potential Recharge Zones in Flinders Ranges, South Australia Using Remote Sensing, GIS, and MIF Techniques. *Water* 2021, 13, 2571. [\[Crossref\]](#).
- Akhter, G.; Hasan, M. Determination of Aquifer Parameters Using Geoelectrical Sounding and Pumping Test Data in Khanewal District, Pakistan. *Open Geosci.* 2016, 8, 630–638. [\[Crossref\]](#).
- Alabi, O.O; Ojo, O.; Akinpelu, D.F. Geophysical Investigation for Groundwater Potential and Aquifer Protective Capacity Around Osun State University (UNIOSUN) College of Health Sciences. *Am. J. Water Resour.* 2016, 4, 137–143.
- Amadi, A.N.; Nwawulu, C.D.; Unuevho, C.I.; Okoye, N.O.; Okunlola, I.A.; Egharevba, N.A.; Ako, T.A.; Alkali, Y.B. Evaluation of the groundwater potential in Pompo Village, Gidan Kwano, Minna using Vertical Electrical Resistivity Sounding. *Br. J. Appl. Sci. Technol.* 2011, 1, 53–66. [\[Crossref\]](#).
- Anbazhagan, S.; Jothibas, A. Geoinformatics in groundwater potential mapping and sustainable development: A case study from southern India. *Hydrol. Sci. J.* 2016, 61, 1109–1123. [\[Crossref\]](#).
- Chinwuko, A. I., Anakwuba, E.K., Okeke, H.C., Usman, A.O., Ovwasa, M.O., & Okoye, I.F. Geo-electric Investigation for Groundwater Potential in Awka, Anambra State, Nigeria. *International Journal of Science for Global Sustainability*, 1(1), 11. 2015. Retrieved from fugus-ijsgs.com.ng.
- Devi, P.D.; Srinivasulu, S.; Raju, K.K. Delineation of groundwater potential zones and electrical resistivity studies for groundwater exploration. *Environ. Earth Sci.* 2001, 40, 1252–1264. [\[Crossref\]](#).
- Eduvie, M.O and Garba, M.L. Appraisal of Groundwater Potential of Fadama Areas within Northern Nigeria: A Review. *Journal of Geoscience and Environment Protection*, 9(1):44-57. 2017. [\[Crossref\]](#).
- Ejebu, S. J. and Olasehinde, P. I. Groundwater potential evaluation in the crystalline basement of Gidan Kwano Campus, Federal University of Technology, Minna, North-Central Nigeria using

- geoelectric methods. *Universal Journal of Geoscience*, 2, (4): 123-132. 2014. [\[Crossref\]](#).
- Hasan, M.; Shang, Y.; Akhter, G.; Jin, W. Geophysical Assessment of Groundwater Potential: A case study from mian Channu Area, Pakistan. *Groundwater* 2018, 56, 783–796. [\[Crossref\]](#).
- Hawker, L., Neal, J., and Bates, P. “Accuracy assessment of the Tan DEM-X 90 Digital Elevation Model for Selected Floodplain Sites”, *Remote Sens Environ*, vol. 232, no. July, pp. 1– 15, 2019. [\[Crossref\]](#)
- Khal, M., Algouti, A., Algouti, A., Akdim, N., and Stankevich, S. A. “Evaluation of Open Digital Elevation Models: Estimation of Topographic Indices Relevant to Erosion Risk in the Wadi M ’ Goun watershed”, vol. 6, no. April, pp. 231– 257, 2020. [\[Crossref\]](#)
- Marere, O. S; Dio, E; Iwhiwhu, S. O. Electrical Resistivity Tomography and Vertical Sounding for Groundwater Potentials in Erhoike Community, Delta State, Nigeria. *J. Appl. Sci. Environ. Manage.* 27 (6) 1189-1192. 2023. [\[Crossref\]](#).
- Nzelibe, I. U., Mogaji, I. N., and Tata, H. Assessing Vertical Accuracies of Satellite-Dem for Terrain Modelling in Akure, Nigeria. *Nigerian Journal of Technology*, 2024; 43(2), pp. 391 – 399. [\[Crossref\]](#)
- Nzelibe, I. U., Ojediran, D. D., and Moses, M. Geospatial Assessment and Mapping of Suitable Sites for a Utility-scale Solar PV Farm in Akure South, Ondo State, Nigeria. *Geomatics and Environmental Engineering*. 16(4): 79–101, 2022. [\[Crossref\]](#)
- Ogilbee, W and Anderson, H.R. Aquifers in the Sokoto Basin, Northwestern Nigeria, With a Description of the General Hydrogeology of the Region. Geological Survey Water-Supply Paper 1757-L. United State Government Printing Office, 1973. 2401-02389pp. pubs.usgs.gov.
- Ojo, J.S.; Olorunfemi, M.O.; Akintorinwa, O.J.; Bayode, S.; Omosuyi, G.O.; Akinluyi, F.O. GIS Integrated Geomorphological, Geological and Geoelectrical Assessment of the Groundwater Potential of Akure Metropolis, Southwest Nigeria. *J. Earth Sci. Geotech. Eng.* 2015, 5, 85– 101. scienpress.com.
- Oladapo, M.; Akintorinwa, O. Hydrogeophysical Study of Ogbese South Western Nigeria. *Glob. J. Pure Appl. Sci.* 2007, 13, 55–61. [\[Crossref\]](#).
- Olorunfemi, MO; Oni, AG. Integrated Geophysical Methods and Techniques for Siting Productive Boreholes in Basement Complex Terrain of Southwestern Nigeria. *Ife J Sci.* 2019, 21: 001– 014. [\[Crossref\]](#).
- Olorunfemi, MO; Oni, AG; Bamidele, O.E; Fadare, TK; Aniko, OO. Combined Geophysical Investigations of The Characteristics of A Regional Fault Zone for Groundwater Development in a Basement Complex Terrain of South-West Nigeria. *SN Appl. Sci.* 2020, 2(6): 1– 17. [\[Crossref\]](#)
- Puttiwongrak, A.; Men, R.; Vann, S.; Hashimoto, K.; Suteerasak, T. Application of Geoelectrical Survey and Time-Lapse Resistivity with Groundwater Data in Delineating a Groundwater Potential Map: A Case Study from Phuket Island, Thailand. *Sustainability* 2022, 14, 397. [\[Crossref\]](#)
- Saad, R.; Nawawi, M.N.M.; Mohamad, E.T. Groundwater Detection in Alluvium Using 2-D Electrical Resistivity Tomography (ERT). Available online: [researchgate.net](https://www.researchgate.net).
- Shuaibu, A.M., Garba, M.L and Abubakar, I.Y. Aquifer Characteristics and Groundwater Flow System in a Typical Basement Complex and Gundumi Formation Northwest, Nigeria. *Bayero Journal of Pure and Applied Sciences.* 14(2): 1 – 7. 2022. [\[Crossref\]](#).
- Shuaibu, A.M., Garba, M.L and Abubakar, I.Y. Geoelectrical Assessment of Groundwater Potential within Zamfara and its Environs, Northwestern Nigeria. *CaJoST*, 2022, 1, 54-70, [\[Crossref\]](#).
- Shuaibu A.M. Structural Analysis, Petrographic Study and Geochemical Assessment of Pan- African Granitoid, Gusau Sheet 54se Northwest Nigeria. *Malaysian Journal of Geosciences*, 2023, 7(1): 50-63. [\[Crossref\]](#).
- Takele Gadissa, Maurice Nyadawa, Benedict Mutua, and Fiseha Behulu, “Comparative Assessment of the Effect of Climate Change and Human Activities on Streamflow Regimes in Central Rift Valley Basin, Ethiopia.” *American Journal of Water Resources*, Vol. 7, no. 1 (2019): 23-29. doi: 10.12691/ajwr-7-1-4.
- Taweelarp, S.; Khebhareon, M.; Saenton, S. Evaluation of Groundwater potential and safe yield of heterogeneous unconsolidated Aquifers in Chiang Mai basin, Northern Thailand. *Water* 2021, 13, 558. [\[Crossref\]](#).
- Vann, S.; Puttiwongrak, A.; Suteerask, T.; Koedsin, W. Delineation of Seawater Intrusion Using Geoelectrical Survey in a Coastal Aquifer of Kamala Beach, Phuket, Thailand. *Water* 2020, 12, 1–14. [\[Crossref\]](#).
- Zhao, J., Huang, S., Huang, Q., Wang, H. and Leng, G., “Detecting the Dominant Cause of Streamflow Decline in the Loess Plateau of China Based on the Latest Budyko Equation,” *Water*, 10 (1277). 2018. [\[Crossref\]](#)